Organic & Biomolecular Chemistry

Accepted Manuscript

ROYAL SOCIETY OF CHEMISTRY

www.rsc.org/obc

Invariom based electron density studies on the C/Si analogues haloperidol/sila-haloperidol and venlafaxine/sila-venlafaxine

Peter Luger,[*a] Birger Dittrich[b] and Reinhold Tacke[*c]

[a]*Institut für Chemie und Biochemie – Anorganische Chemie, Freie Universität Berlin, Fabeckstraße 36a, D-14195 Berlin, Germany. E-mail: lugerp@zedat.fu-berlin.de*

[b]*Institut für Angewandte und Anorganische Chemie, Universität Hamburg, Martin-Luther-King-Platz 6, D-20146 Hamburg, Germany*

[c]*Institut für Anorganische Chemie, Universität Würzburg, Am Hubland, D-97074 Würzburg, Germany. E-mail: r.tacke@uni-wuerzburg.de*

Abstract

Subject of this study are the structures and electron densities of the carbon/silicon analogues haloperidol/sila-haloperidol (**1a**/**1b**) and venlafaxine/sila-venlafaxine (**2a**/**2b**). The parent carbon compounds **1a** (an antipsychotic agent) and **2a** (an antidepressant) are both in clinical use. For haloperidol/sila-haloperidol, three published structures were studied in more detail: the structures of haloperidol hydrochloride (**1a**·HCl), haloperidol hydropicrate (**1a**·HPic) and sila-haloperidol hydrochloride (**1b**·HCl). For venlafaxine/sila-venlafaxine, the published structures of venlafaxine (**2a**), venlafaxine hydrochloride (**2a**·HCl; as orthorhombic (**2a**·HCl-ortho) and monoclinic polymorph (**2a**·HCl-mono)) and sila-venlafaxine hydrochloride (**2b**·HCl) were investigated. Based on these structures, the molecular electron densities were reconstructed by using the invariom formalism. They were further analysed in terms of Bader's quantum theory of atoms in molecules, electrostatic potentials mapped onto electron density isosurfaces and Hirshfeld surfaces. These studies were performed with a special emphasis on the comparison of the corresponding carbon/silicon analogues.

---

*Electronic supplementary information (ESI) available: Bond critical points; atomic properties (charges and volumes); atomic coordinates, displacement parameters and multipole parameters for the haloperidol/sila-haloperidol structures (**1a**·HCl), (**1a**·HPic), (**1b**·HCl) and the venlafaxine/sila-venlafaxine structures (**2a**), (**2a**·HCl), (**2a**·HCl-ortho), (**2b**·HCl).*

Introduction

Starting with the first pioneering studies on biologically active organosilicon compounds five decades ago, silicon chemistry is nowadays an established source of chemical diversity in drug design, with quite promising perspectives.[1] Sila-substitution (carbon/silicon switch, carbon/silicon exchange) is one of the strategies that have been successfully used for the development of new silicon-based drugs.[2] Based on this strategy, some years ago we have synthesized the silicon analogues of the dopamine D_2 antagonist haloperidol (**1a**) and the serotonin/noradrenaline reuptake inhibitor venlafaxine (**2a**), sila-haloperidol (**1b**) and sila-venlafaxine (**2b**), and have evaluated the biological properties of these compounds (Fig.1).[3,4] As analogous alcohols of the formula type R_3COH (R = organyl) differ from the analogous silanols R_3SiOH both in their chemical and physiochemical properties, replacement of the R_3COH carbon atom of **1a** and **2a** by a silicon atom was very promising, because the OH groups of **1a** and **2a** are pharmacophoric groups

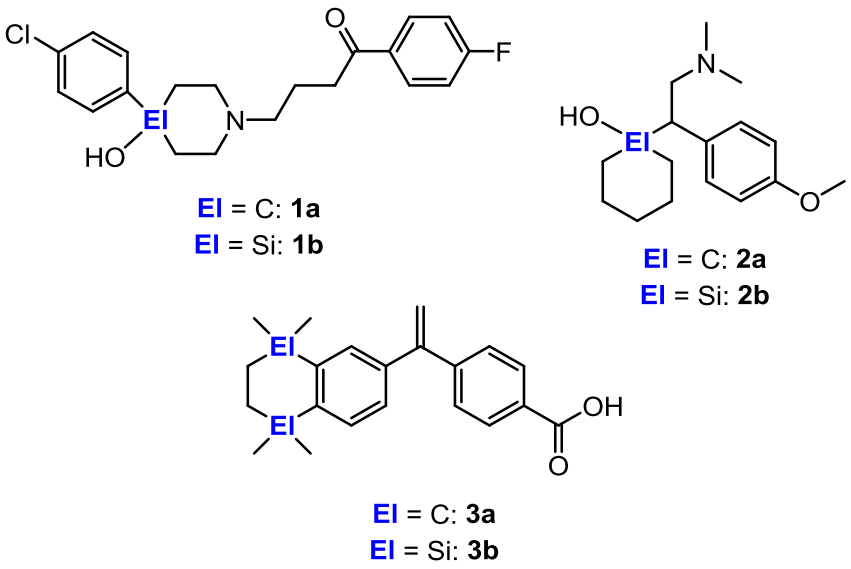

Fig. 1 Chemical structures of haloperidol (**1a**), sila-haloperidol (**1b**), venlafaxine (**2a**), sila-venlafaxine (**2b**), bexarotene (**3a**) and disila-bexarotene (**3b**).

Haloperidol (**1a**), which was developed in the late 1950s,[5] is an antipsychotic agent that is still in clinical use for the treatment of schizophrenia, although it may cause severe extrapyramidal side effects, including parkinsonism and tardive dyskinesia.[6] The pyridinium-type metabolite HPP^+ was proposed to contribute to these neurotoxic side effects.[7] As shown by radioligand binding studies at all five human dopamine receptor subtypes, the silicon analogue sila-haloperidol (**1b**) shows a 5-fold higher affinity for hD_2 receptors than haloperidol (**1a**) itself, whereas the C/Si analogues **1a** and **1b** are approximately equipotent at all the other dopamine receptors (differences are less than 2-fold).[3b] As a result, the subtype selectivity of the silicon compound **1b** for hD_2 over the other

dopamine receptors is higher than that of the parent carbon compound **1a**. Functional studies at hD_1 and hD_2 receptors revealed similar results.[3c] As shown by studies in human and rat liver microsomes and hepatocytes, the metabolic fate of haloperidol (**1a**) and sila-haloperidol (**1b**) is quite different.[3b,d] Most importantly a silicon analogue of the neurotoxic metabolite HPP^+ is not formed in the metabolism of **1b**; instead, two silanediols were detected.

Racemic venlafaxine (**2a**) is in clinical use as an antidepressant.[8] Sila-substitution of **2a** was found to dramatically influence the pharmacological selectivity profile with respect to serotonin, noradrenaline, and dopamine reuptake inhibition. Upon C/Si exchange, the potency at serotonin transporters is reduced by approximately 2 orders of magnitude, whereas a small increase in potency was observed at the noradrenaline and dopamine transportes.[4b] Thus, the pharmacological selectivity profile of the silicon compound **2b** was not suitable for its further development as an antidepressant. Instead, (*R*)-sila-venlafaxine ((*R*)-**2b**), a selective noradrenaline reuptake inhibitor, was preclinically developed as a drug for the treatment of emesis.[4c,d] Interestingly, the carbon analogue (*R*)-venlafaxine ((*R*)-**2a**) is a selective serotonin/noradrenaline reuptake inhibitor.[4b]

To understand the changes of the pharmacological selectivity profiles upon sila-substitution of **1a** and **2a**, we were interested to get some more information about the similarities and dissimilarities of the respective C/Si analogues on the molecular level. We have recently examined the similarities/dissimilarities of the retinoid agonists bexarotene (**3a**) and disila-bexarotene (**3b**) (Fig.1) on the level of their molecular electron density distribution (EDD),[9] which provides information about ligand–receptor interaction on an atomic scale beyond the structure, i.e., connectivity, bond lengths and angles. The invariom formalism[10,11] provides the EDD and derived properties with only moderate effort, and we have therefore extended our investigations and have studied the EDD of the C/Si pairs **1a**/**1b** and **2a**/**2b**.

Invariom refinement and analysis of the electron density

For the C/Si pair haloperidol/sila-haloperidol (**1a**/**1b**), we made use of the known crystal structures of haloperidol hydrochloride (**1a**·HCl, CSD access code BIDFUQ[12]),[3a] haloperidol hydropicrate (**1a**·HPic, CUCYUV[12])[13] and sila-haloperidol hydrochloride (**1b**·HCl, BIDGAX[12]).[3a] In contrast to the neutral bexarotene (**3a**) and disila-bexarotene (**3b**) molecules studied before,[9] compounds **1a**·HCl, **1a**·HPic and **1b**·HCl are salts, i.e., they contain protonated haloperidol or sila-haloperidol as the cation in their solid-state structures. These three structures allow to compare the properties of (i) the two C/Si-analogous cations (protonated haloperidol versus protonated sila-haloperidol) and (ii) protonated haloperidol in the presence of two different counterions (chloride versus picrate).

For the C/Si pair venlafaxine/sila-venlafaxine (**2a**/**2b**), we investigated four published data sets obtained from single-crystal X-ray diffraction experiments: venlafaxine (**2a,** OCALAG[12]) itself,[14] two polymorphs of venlafaxine hydrochloride (**2a**·HCl) in orthorhombic (**2a**·HCl-ortho, WOBMUV[12])[15] and monoclinic form (**2a**·HCl-mono, WOBMUV01[12])[16] and sila-venlafaxine hydrochloride (**2b**·HCl, GEDBIB[12]).[4b] The data sets used refer to the respective racemates. These four structures allow to compare the properties of (i) the neutral venlafaxine (**2a**) molecule with the two ionic forms **2a**·HCl-ortho and **2a**·HCl-mono, (ii) the two chemically identical salts **2a**·HCl-ortho and **2a**·HCl-mono in different crystal systems (orthorhombic versus monoclinic) and (iii) the cations of the two forms of venlafaxine hydrochloride (**2a**·HCl-ortho and **2a**·HCl-mono) with the cation of the silicon analogue sila-venlafaxine hydrochloride (**2b**·HCl).

The invariom formalism and the corresponding data base of aspherical scattering factors were applied. It relies on the Hansen & Coppens 'multipole' scattering-factor model.[17] The procedure was similar to that described in some more detail in reference 9, except that bond distances to hydrogen atoms were elongated to values from energy minimized structures of the respective model compounds also used in scattering-factor assignment. Hydrogen positions were idealized and constrained in a riding model; constraints were generated with the preprocessor program *InvariomTool*.[18] After invariom transfer, refinement of positional and anisotropic displacement parameters for non-hydrogen atoms was carried out making use of the *XD2006* program suite.[19] In the case of the salt structures, full charge transfer was assumed, and the chlorine atom was treated as a chloride anion.

Special attention had to be payed to the invariom assignment for the disordered picrate in the structure of **1a**·HPic, which was carried out with the program *MoleCoolQt*.[20] It is a quite novel aspect that has so far not been well covered in the literature to model (partially) disordered structures with invarioms, although case studies with disordered solvent or side-chain disorder were already published.[21] In principle the procedure is straightforward. Initially the invariom scattering factor names of all atoms in a structure need to be known and assigned also to the disordered atoms. This can be done manually when there is only minor disorder, but it becomes impractical for larger disordered molecules. Then the density-normalized multipole populations that describe the devation of valence electron density from a spherically symmetric distribution need to be modified. Disorder modelled with split occupancies already provides partial atomic occupancy parameters, and these then need to be multiplied with the DFT-derived multipole parameters of the invariom database. In the XD program such populations might already be a fraction of unity when an atom resides on a special position, and if applicable this also needs to be taken into account. A publication that reports

on the tools that we have developed to facilitate the practical procedure using the example of a severely disordered cephalosporin antibiotic is in preparation.

Selected crystallographic and refinement data are summarized in Table 1 (for **1a**·HCl, **1a**·HPic and **1b**·HCl) and Table 2 (for **2a**, **2a**·HCl-ortho, **2a**·HCl-mono and **2b**·HCl). In a next step, the molecular EDDs obtained in these studies were evaluated by topological analysis according to Bader's quantum theory of atoms in molecules (QTAIM formalism),[22] using the subprogram *XDPROP* of *XD2006*.[19]

Results and discussion

Structural properties

The molecular structures of **1a**·HCl, **1a**·HPic and **1b**·HCl as well as **2a**, **2a**·HCl-ortho, **2a**·HCl-mono and **2b**·HCl are displayed in ORTEP[23] representations in Figs. 2 and 3, respectively, generated with PLATON.[24] Atomic numbering schemes from the original publications (refs. 3a and 13 for **1a**·HCl, **1a**·HPic and **1b**·HCl; refs. 4b and 14–16 for **2a**, **2a**·HCl-ortho, **2a**·HCl-mono and **2b**·HCl) were maintained. Therefore, atom numbering for **1a**·HCl and **1b**·HCl are identical, but differ from that of **1a**·HPic, and the structures of **2a**·HCl-ortho and **2a**·HCl-mono agree in their atom numbering, but not with **2a** or **2b**·HCl.

Haloperidol/sila-haloperidol

Since the bond lengths and angles determined do not provide additional information compared to that discussed in refs. 3a and 13, they will not be commented on further. However, some details concerning the molecular conformations shall be mentioned.

In all three structures, the piperidinium/silapiperidinium ring has a chair conformation, with the hydroxyl oxygen atom in an axial and the *N*-organyl group in an equatorial position. The already reported flattening of the silapiperidinium ring of **1b**·HCl[3a] compared to the piperidinium rings of **1a**·HCl and **1a**·HPic is expressed quantitatively by the endocyclic torsion angles around the Si–C bonds, which are close to ± 44°. This value is more than 10° smaller than that for the corresponding C–C torsion angles of **1a**·HCl and **1a**·HPic.

The inclination of the chlorophenyl ring with respect to the piperidinium/silapiperidinium ring as quantified by the torsion angle C8–C7–C1–C13 (or equivalent numbering in **1a**·HPic) is alike in **1a**·HPic and **1b**·HCl (torsion angles 127.8(2)° and 130.4(2)°, respectively) but different compared

with **1a**·HCl (torsion angle 75.8(2)°). The major conformational difference is seen along the bond C18–C19 (or equivalent numbering in **1a**·HPic). The torsion angle C17–C18–C19–C20 is –164.1(1)° for **1a**·HCl, –82.6(2)° for **1a**·HPic and 71.8(2)° for **1b**·HCl, so that pronounced conformational flexibility exists along this bond. It follows that the molecular structures of the cations of compounds **1a**·HCl, **1a**·HPic and **1b**·HCl are quite different.

Venlafaxine/sila-venlafaxine

In this section, we also confine only to the discussion of the molecular conformations. For the cyclohexane/silacyclohexane chair the same ring flattening for the silicon compound **2b**·HCl is observed as already discussed for the C/Si analogues **1a**·HCl and **1b**·HCl, with small endocyclic torsion angles at the Si–C bonds close to ± 45°. The overall conformational situation for **2a**, **2a**·HCl-ortho, **2a**·HCl-mono and **2b**·HCl can almost completely be described by the torsion angles around the five bonds N1–C3, C3–C4, C4–C5, C4–C11 and C14–O2 (atom numbers refer to the numbering scheme used for **2a**; see Fig. 3a). Compounds **2a**·HCl-ortho and **2a**·HCl-mono are conformationally equal, and comparable torsion angles differ by no more than 10°. Likewise, the conformation of **2b**·HCl is similar to those of **2a**·HCl-ortho and **2a**·HCl-mono, except for the orientation of the dimethylammonio group, where the torsion angles around the N1–C3 and C3–C4 bonds in **2b**·HCl differ considerably from those of **2a**·HCl-ortho and **2a**·HCl-mono.

The conformation of the tertiary amine **2a** is completely different to those of the ammonium salts **2a**·HCl-ortho, **2a**·HCl-mono and **2b**·HCl. This is due to an intramolecular hydrogen bond in **2a** discussed below, which is not present in the ammonium salts. It follows that the molecular structures of the ammonium cations of **2a**·HCl-ortho, **2a**·HCl-mono and **2b**·HCl are similar, but completely different from that of the tertiary amine **2a**.

Intermolecular interactions

Hydrogen bonds between the ammonium cation and the counterion exist in all three haloperidol/sila-haloperidol structures studied (**1a**·HCl, **1a**·HPic and **1b**·HCl; Fig. 4, Table 3). The hydrogen bonds are OH···Cl and NH···Cl interactions for **1a**·HCl and **1b**·HCl and OH···O and NH···O contacts to oxygen atoms of the picrate anion of **1a**·HPic. In the case of **1a**·HCl and **1b**·HCl, atom sequences O–H···Cl···H–N lead to infinite chains of cations linked to their chloride counterions. In the case of **1a**·HPic, O–H···O–N–O···H–N interactions also lead to infinite chains of cations linked to the picrate counterion, where the twofold acceptor fragment O–N–O is one of the three nitrato groups of the picrate anion, and the N–H donor group of the piperidinium ring forms a bifurcated hydrogen bond with a neighbored oxygen atom of the picrate anion as a second acceptor. The special

conformational situation at the bond C18–C19 of **1a**·HCl allows an additional (weak) C–H···O contact to the adjacent cation.

A summary of the hydrogen bonding topologies for the venlafaxine/sila-venlafaxine structures (**2a, 2a**·HCl-ortho, **2a**·HCl-mono and **2b**·HCl) is given in Fig. 5 and Table 4. An intramolecular O1–H1···N1 hydrogen bond exists in the neutral tertiary amine **2a**, whereas in the ammonium salts **2a**·HCl-ortho, **2a**·HCl-mono and **2b**·HCl intermolecular O–H···Cl and N–H···Cl hydrogen bond establish O–H···Cl···H–N bridging sequences via the chloride counterion, leading to infinite chains of cations linked by their chloride counterions.

Hence, in all cases where chloride is the counterion (**1a**·HCl, **1a**·HPic, **1b**·HCl, **2a**·HCl-ortho, **2a**·HCl-mono, **2b**·HCl), the pattern of intermolecular interaction is basically the same.

Bond topological and atomic properties

The molecular EDD of the title compounds as reconstructed from invariom fragments was subjected to a quantitative analysis according to Bader's QTAIM formalism.[22] This analysis provides both bond critical points (BCPs, defined by the property that the gradient $\nabla\rho(\mathbf{r})$ vanishes at this point) and atomic properties by integration over the atomic basins bound by the zero flux surfaces of the gradient vector field, which subdivide a structure into transferable substructures.

BCPs were located on all covalent bonds and on the H(donor)···X(acceptor) (X = Cl, O) linkages of the hydrogen bonds. ED values, Laplacians and ellipticities [$\rho(\mathbf{r}_{BCP})$, $\nabla^2\rho(\mathbf{r}_{BCP})$, ε], which provide information about the strength and nature of a bond, are summarized in Tables 5 and 6. It turned out, that – as expected – the obtained quantities are practically the same for comparable bond types so that only averages for the structures of **1a**·HCl, **1a**·HPic and **1b**·HCl are listed in Table 5, while averages for the structures of **2a, 2a**·HCl-ortho, **2a**·HCl-mono and **2b**·HCl are given in Table 6. Detailed lists for all seven compounds are provided in the ESI (Tables S1–S7). Moreover, inspection of Tables 5 and 6 indicates a close agreement in all bond topological properties of comparable bonds of all compounds studied.

If the central carbon atom in **1a**·HCl/**1a**·HPic or **2a**·HCl-ortho/**2a**·HCl-mono is replaced by a silicon atom (→**1b**·HCl or **2b**·HCl), the following changes in bond topological properties are observed: for the longer Si–C and Si–O bonds (compared to the analogous C–C and C–O bonds), the ED values are much lower. For the Si–C bonds, the values of $\rho(\mathbf{r}_{BCP})$ and $\nabla^2\rho(\mathbf{r}_{BCP})$ are comparable to those reported for disila-bexarotene (**3b**),[9] except that the Laplacian was slightly negative in **3b** but is positive in the present cases. However, it was already noted that this is insignificant because the

Laplacian along the Si–C bond has a steep slope close to the BCP and can easily change the sign in its vicinity as illustrated in Fig. 6 for **2b**·HCl. For the Si–O bonds in **1b**·HCl and **2b**·HCl, the Laplacians of +17.3 and +16.8 e Å^{-5} are strongly positive. Si–O bonds were recently examined in detail by experiment and theory.[25–27] The $\rho(\mathbf{r}_{BCP})$ values of the Si–O bonds reported were in the range 0.86 to 0.97 e Å^{-3}; the corresponding Laplacians were +16.0 to +25.2 e Å^{-5} and are therefore in the same range as in **1b**·HCl and **2b**·HCl. This means that the Si–O bond has a highly ionic character. Fig. 6 shows the Laplacians along the non-polar C8–C7 and the polar C8–O2 bond in **2a**·HCl-ortho and the analogous Si–C6 and Si–O1 bonds in **2b**·HCl to illustrate their different character.

Atomic properties were calculated by integration over the atomic basins described above. The algorithm provided by *XDPROP*[19] was used which was introduced by Volkov et al.[28]. Since Bader volumes and charges are additive it can easily be checked whether the calculation has worked properly. The atomic charges should sum up to the total charge of the considered species (e.g. zero in the neutral or +1 in the cationic case) and the sum of the atomic volumes multiplied by Z should reproduce the unit cell volume. This was fulfilled in all cases so that the integrations were accepted as correct.

A selection of atomic volumes and charges for **1a**·HCl, **1a**·HPic and **1b**·HCl is given in Table 7 and for **2a, 2a**·HCl-ortho, **2a**·HCl-mono and **2b**·HCl in Table 8. Only those atoms are listed where $|q| > 0.15$ e for one of the contributing structures (a complete list is given in the ESI; Tables S8 - S14). We note that for the hydrogen atoms only the two atoms involved in hydrogen bonding carry significant (positive) charges.

All three haloperidol/sila-haloperidol structures (**1a**·HCl, **1a**·HPic and **1b**·HCl) contain strongly negative centers at the two oxygen and at the piperidinium nitrogen sites, with charges close to –1 e. A moderately negative charge is found at the fluorine atom, whereas the second halogen atom at the chlorophenyl ring has only a rather small negative charge. While the atomic properties of **1a**·HCl and **1a**·HPic are very much alike, they are different from those of **1b**·HCl in that the silicon atom exhibits a strongly positive charge with $q \approx +3$ e. An Si atomic charge close to +3 e looks quite unexpected. However, there are examples in the literature supporting his finding. Already in 1998 Pedersen et al. have reported an Si charge of +3.35 e for a silatran derivative commented by these authors that this value is “somewhat counterintuitive”.[29a] The Bader formalism was also applied by Grabowsky et al. on a number of Si derivatives.[25,27] They made use of high resolution X-ray experimental data and periodic and non periodic theoretical calculations and came to Si atomic charges in a range of +2.5 to +3.0 e. Experimental and theoretical ED studies on Si compounds with large positive Bader charges of Si (e. g. +2.78 from experimental ED and +3.13 e from a B3LYP/6-311G** calculation) were also reported by Kocher et al.[29b] and Ott et al.[29c]. In none of the above

mentioned references the invariom formalism was applied so that this aspect has obviously no influence on the Si charge.

The abovementioned strongly negative charges are compensated by the adjacent covalently bound atoms. The piperidinium nitrogen atom for example carries a charge of –0.91/–0.81/–0.91 e in **1a**·HCl/**1a**·HPic/**1b**·HCl, whereas the sum of the charges of the four direct neighbor atoms is +1.11/+1.10/+1.07 e. Hence, only an excess charge of 0.16–0.29 e is distributed in the environment of the nitrogen atom.

The atomic properties of the four venlafaxine/sila-venlafaxine structures (**2a, 2a**·HCl-ortho, **2a**·HCl-mono and **2b**·HCl; Table 8) can be discussed in the same manner as for the haloperidol/sila-haloperidol structures. Negative charges are found for hydroxyl and methoxy oxygen atoms and the nitrogen atom of the dimethylamino/dimethylammonio group. In the neutral tertiary amine **2a**, the nitrogen atom carries a Bader charge of –0.81 e, while the sum of the charges of the three neighboring carbon atoms is +0.67 e, so that a small charge of –0.14 e remains. The situation is somewhat different for the ammonium salts **2a**·HCl-ortho, **2a**·HCl-mono and **2b**·HCl, where the average charge at the nitrogen atoms is –0.88 e and that of the four nitrogen-bound atoms (including HN) is +0.20 e, hence slightly positive and comparable to the finding for **1a**·HCl, **1a**·HPic and **1b**·HCl. There is also a significant difference in the volume of the nitrogen atom in the neutral and cationic form: in the neutral tertiary amine **2a**, the atomic volume is by 1.5 Å larger than in the ammonium salts **2a**·HCl-ortho, **2a**·HCl-mono and **2b**·HCl. As observed for **1b**·HCl, the silicon atom of **2b**·HCl has a strongly positive charge.

Molecular surfaces

In mutual drug–receptor recognition processes involving pharmacologically relevant molecules, molecular surfaces and the corresponding surface properties play an important role. That is why we consider both the electrostatic potential (ESP) mapped onto an EDD isosurface and the Hirshfeld surface:

(i) The ESP was calculated by using the method of Volkov et al.[30] with the *XDPROP* subprogram of *XD2006*[19] and colour coded onto the 0.0067 e Å^{-3} (= 0.001 a.u.) EDD isosurface (see Figs. 7–10).[31] The study of the ESP is very helpful for understanding molecular polarization and reactivity behavior.

(ii) The Hirshfeld surface[32,33] is defined by the ratio of the molecular EDD versus the crystal density when equal to 0.5. When the aspherical EDD is mapped by a colour code onto

this surface, EDD concentrations are emphasized so that sites and strengths of intermolecular interactions become visible (see Figs. 11 and 12).[31]

The ESP surfaces of the ammonium cations of **1a**·HCl, **1a**·HPic and **1b**·HCl are displayed in Fig. 7. All three cationic structures have in common a polarization between the central region around the piperidinium/silapiperidinium fragment, with the strongest positive ESP, and the terminal *p*-chloro- and *p*-fluorophenyl rings, where the ESP is less positive. The ESP distribution supports findings regarding the atomic charges around the nitrogen atom as discussed above, in that the formal charge of +1 e of the cation is distributed over a larger range of the neighbored atoms. This was also observed earlier by a multipole refinement with high-resolution X-ray diffraction data of a protonated opioid derivative.[34]

The ESP distributions for the cations of **1a**·HCl and **1a**·Pic (Figs. 7a and 7b) are rather alike and compare well also with the major features of **1b**·HCl (Fig. 7c). However, a detailed inspection of Fig. 7c reveals that the carbon environment of the silicon atom of **1b**·HCl looks somewhat different. This is emphasized in the surface of the difference potential between **1b**·HCl and **1a**·HCl as shown in Fig. 8. Note that the figure legend indicates only a small potential difference of less than 0.1 e $Å^{-1}$, which is however exclusively located in a torus shaped region around the silicon atom. Outside this region the difference potential is zero.

The ESP distributions for **2a**, **2a**·HCl-ortho and **2b**·HCl are displayed in Fig. 9. The neutral molecule **2a** has two negative surface regions around the oxygen atoms, a rather extended region at the methoxy oxygen atom and a smaller localized region at the hydroxyl oxygen atom (Fig. 9a); otherwise, the ESP surface is positive. The ESPs of **2a**·HCl-ortho and **2a**·HCl-mono are equal within the graphical error, so that only the ESP of **2a**·HCl-ortho is shown (Fig. 9b). The surface region around the nitrogen atom is the most positive one, which is not true for the silicon analogue **2b**·HCl (Fig. 9c). As a consequence, a negative region around the silicon atom is seen in the difference potential **2b**·HCl minus **2a**·HCl-ortho as shown in Fig. 10. The difference potentials in Figs. 8 and 10 are obtained by subtraction of very similar quantities, so that a more detailed quantitative interpretation does not seem justified.

The Hirshfeld surfaces of **1a**·HCl, **1a**·Pic and **1b**·HCl are depicted in Fig. 11. The darkest colour is indicative of EDD concentrations, which coincide with the donor and acceptor sites of the hydrogen bonds listed in Table 3. Neither for **1a**·Pic nor **1b**·HCl further EDD concentrations are visible. For **1a**·HCl, the weak C–H···O linkage is seen as an EDD concentration of medium strength above the hydrogen atom of the donor carbon atom C15 and at the acceptor oxygen atom O2. A further EED concentration above the terminal fluorine atom results from a short F···F contact of 2.627 Å (van der Waals radius of fluorine: 1.47 Å)[35] between two molecules related via a

crystallographic inversion center. Comparable non bonded F···F contacts shorter than the van der Waals distance have been reported earlier and examined on the basis of the electron density.[36,37] Another nonnegligible EDD concentration above one of the hydrogen atoms at C17 is caused by a weak contact to the chloride anion. Thus, EDD mapped onto the Hirshfeld surface is a very fine probe to recognize all intermolecular contacts in a crystal structure at one glance, whereas some of them might easily be overlooked in an analysis based on geometric criteria.

Intermolecular contacts of the venlafaxine/sila-venlafaxine structures are also visible on Hirshfeld surfaces as shown in Fig. 12, where coloured sites for the ammonium salts **2a**·HCl-ortho, **2a**·HCl-mono and **2b**·HCl again indicate charge concentrations caused by the intermolecular contacts as discussed before (Figs. 12b and 12c). Consequently, the Hirshfeld surface of the tertiary amine **2a** (Fig. 12a) is almost featureless, and the very weak signals are due to weak C–H···O contacts around 2.65 Å. The Hirshfeld surfaces of **2a**·HCl-ortho and **2a**·HCl-mono are practically identical, so that only the illustration for **2a**·HCl-mono is shown (Fig. 12b). The only two strong EDD concentrations are found at the O–H and N–H donor sites. The same features are seen for the Hirshfeld surface of the silicon analogue **2b**·HCl (Fig. 12c), where some additional weak signals indicate C–H···Cl contacts around 2.7–2.9 Å.

Conclusion

The electron density distribution of three haloperidol/sila-haloperidol (**1a**·HCl, **1a**·HPic, **1b**·HCl) and four venlafaxine/sila-venlafaxine (**2a**, **2a**·HCl-ortho, **2a**·HCl-mono, **2b**·HCl) structures as provided by the invariom formalism was investigated. Although there is some conformational flexibility in the ammonium cations, the dominant intermolecular interactions are alike and consist of infinite cation···counterion···cation··· chains. Only in the case of **1a**·HCl an additional weak C–H···O contact between two cations exists. In the neutral tertiary amine **2a,** only an intramolecular O–H···N hydrogen bond is present. Hirshfeld surfaces make strong as well as weak intermolecular interactions visible and can therefore serve as a convenient tool for recognizing the influence of the entire crystal environment of a chemical system. The bond topological properties for the chemically comparable bonds agree well, except for the C–X/Si–X bonds (X = C, O). Pronounced differences between the carbon compounds and their corresponding silicon analogues (**1a**·HCl/**1a**·HPic versus **1b**·HCl and **2a**/**2a**·HCl-ortho/**2a**·HCl-mono versus **2b**·HCl) are seen for the integrated atomic Bader charges. In all ammonium cations and in the neutral tertiary amine, the oxygen and nitrogen atoms are strongly negative centres. For the silicon compounds **1b**·HCl and **2b**·HCl, an additional positive centre at the silicon atom is found (Si atomic charge ≈ +3 e). Although these atomic charge distributions indicate some differences in the electronic structures of the C/Si analogues, the major

features of polarization between the central piperidinium/silapiperidinium fragment and the terminal *p*-chloro- and *p*-fluorophenyl rings in the electrostatic potentials look similar for **1a**·HCl, **1a**·HPic and **1b**·HCl. Only the electrostatic difference potential of **1b**·HCl and **1a**·HCl makes a significant nonzero region visible around the site where the central carbon atom of **1a**·HCl is replaced by a silicon atom (→**1b**·HCl). In case of the venlafaxine/sila-venlafaxine structures, the neutral tertiary amine **2a** completely differs from the ammonium salts **2a**·HCl-ortho, **2a**·HCl-mono and **2b**·HCl concerning conformation and electronic structure. The two ammonium cations of **2a**·HCl-ortho and **2a**·HCl-mono are conformationally and electronically equal. However, as also observed for the C/Si analogues **1a**·HCl and **1b**·HCl, there is a small but significant difference between the electrostatic potential of **2a**·HCl/ **2a**·HPic and the silicon analogue **2b**·HCl, visible as a negative region around the silicon atom in the difference potential.

As the C/Si analogues haloperidol/sila-haloperidol (**1a**/**1b**) and venlafaxine/sila-venlafaxine (**2a**/**2b**) differ in their pharmacological potency and selectivity, the respective ligand–receptor interactions must be different. From the structural and electronic properties derived from this study, two major effects could be responsible for this: differences in the conformational flexibility and/or differences in the electrostatic potentials in the neighborhood of the C/Si replacement site. While the relevant structural parameters of the title compounds were already obtained from conventional X-ray diffraction analyses, the invariom formalism based on these crystal structure analyses additionally provides the electronic structures, which allow a more detailed analysis of the mutual recognition of receptors and their ligands.

A novel aspect of this work was to exploit the major advantage of modeling disorder using theoretically predicted aspherical scattering factors rather than freely refined multipole populations. Since the latter would correlate with split occupancies, thereby invalidating the electron density model, the invariom model was successfully applied to a disordered structure, the picrate anion in **1a**·HPic.

Finally, the question should be commented whether the results from an invariom approach can compete with those obtained from multipole refinement against high resolution X-ray data at low temperatures. This has been examined before in a comparative study on sucrose,[38a] where an invariom modelling of a room temperature low order data set (d = 0.85 Å) was compared with a multipole refinement of a 20 K high resolution data set (d = 0.43 Å).[38b] It was shown that there is an agreement of bond topological and atomic properties in the range of earlier introduced experimental transferability indices (found to be 0.09 e Å^{-3} and 2.8 e Å^{-5} for the ED's and the Laplacians at the bond critical points and 0.7 Å^3 and 0.11 e for the atomic volumes and charges).[38c] Hence, it can be

concluded that the quantitative findings of the invariom application data are reliable within the transferability indices quoted above.

(a)

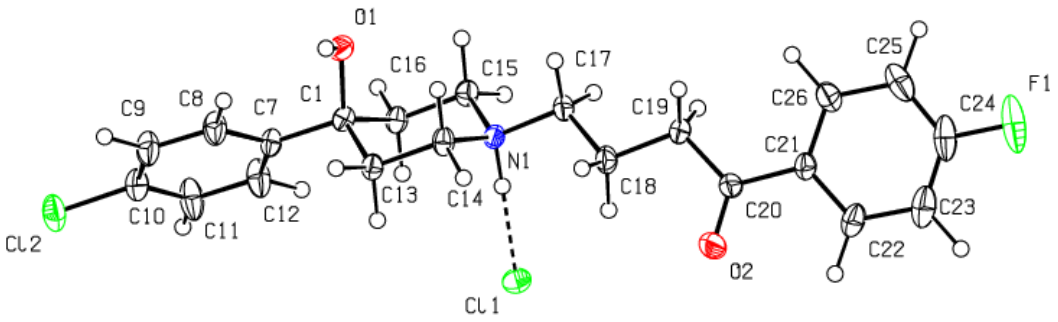

(b)

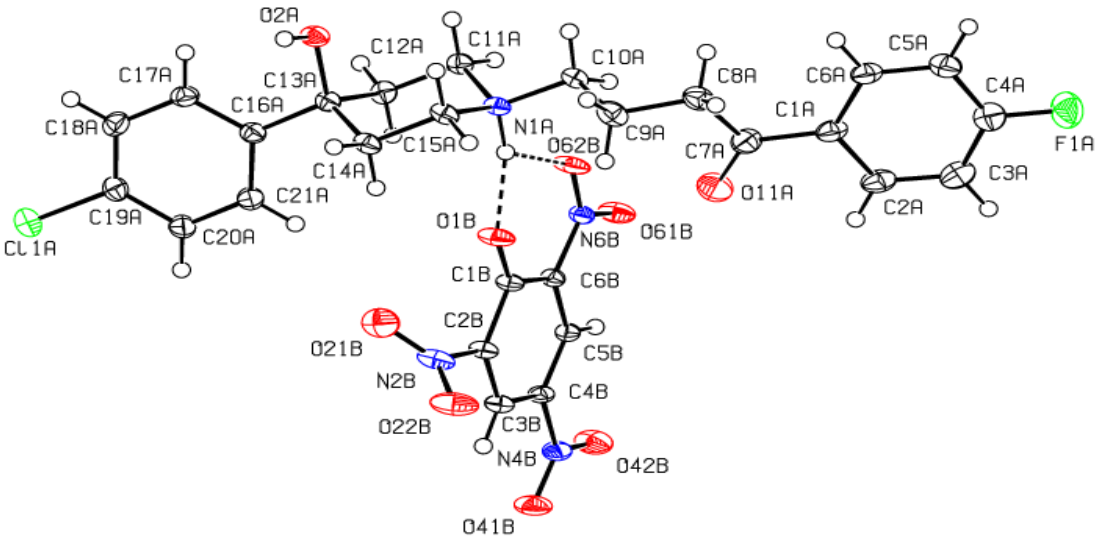

(c)

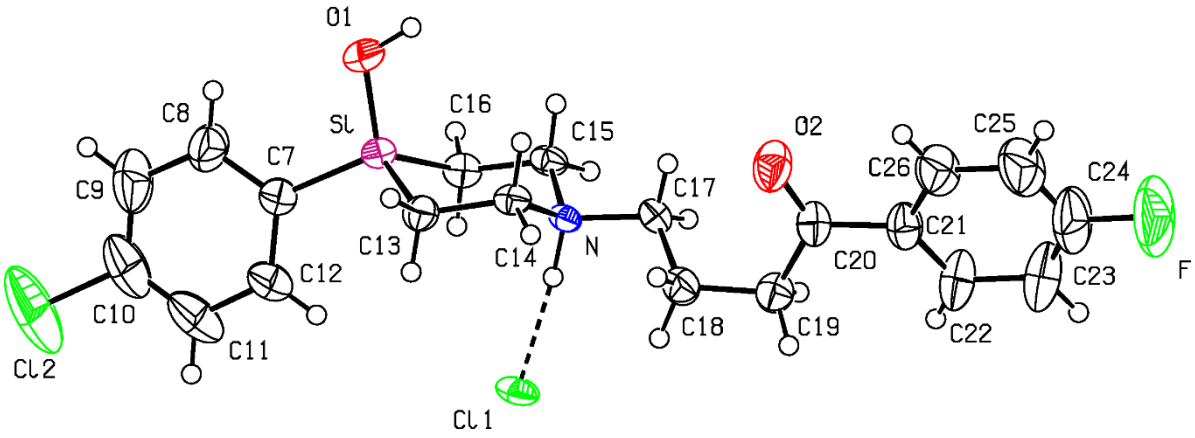

Fig. 2 ORTEP[23] representation[24] of the molecular structures of **1a**·HCl (a), **1a**·HPic (b) and **1b**·HCl (c) with their counterions. The used atomic numbering schemes are also shown.

(a)

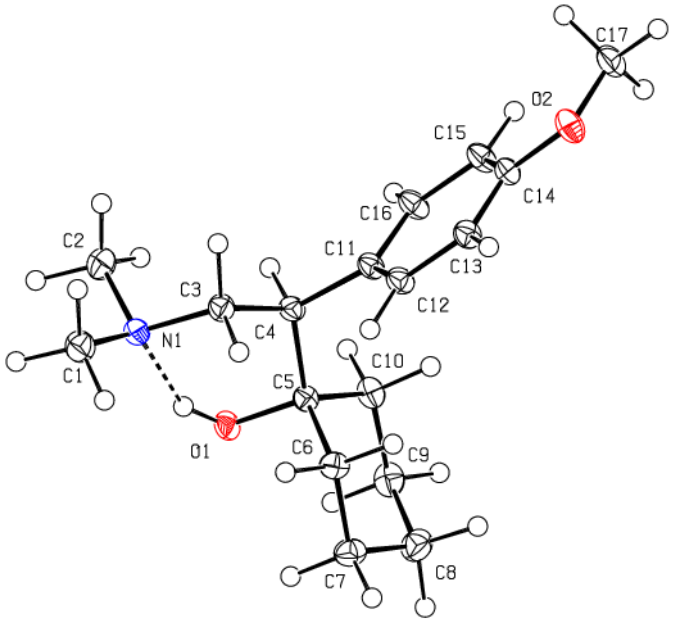

(b)

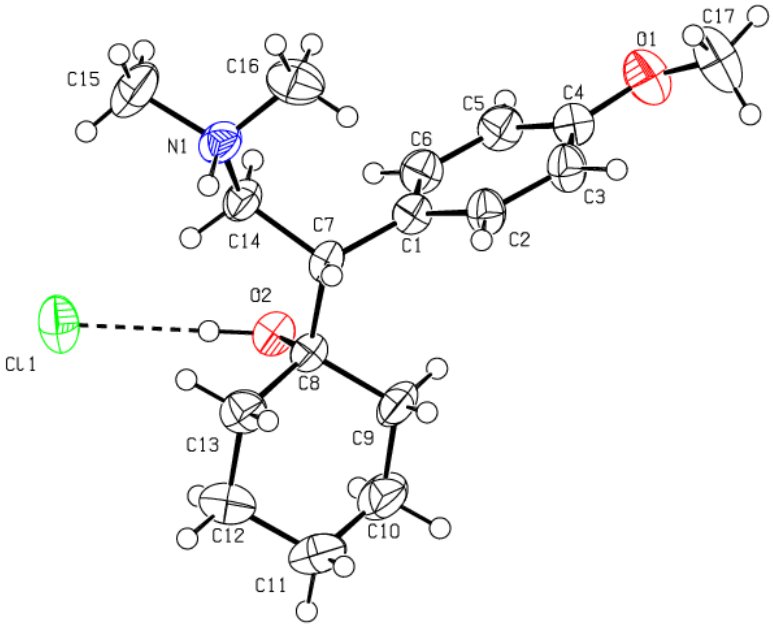

(c)

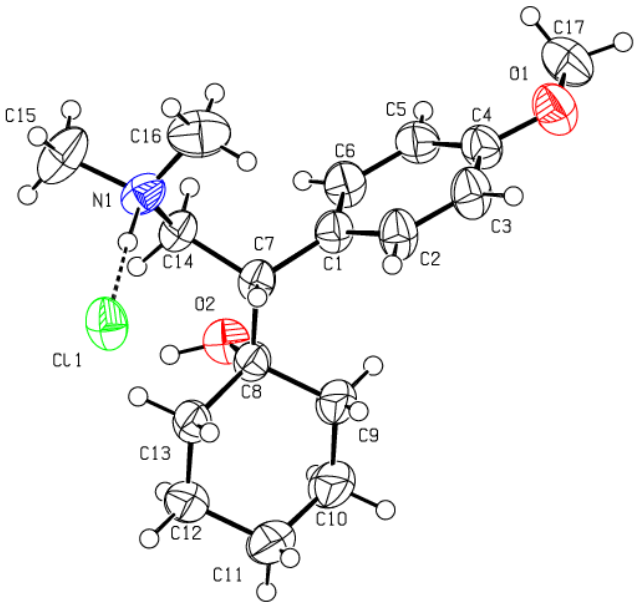

(d)

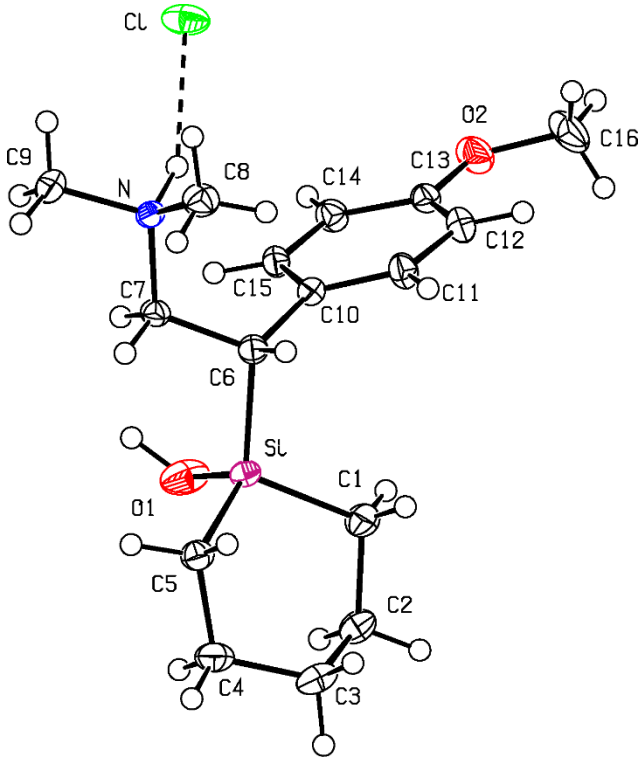

Fig. 3 ORTEP[23] representation[24] of the molecular structures of **2a** (a), **2a**·HCl-ortho (b), **2a**·HCl-mono (c) and **2b**·HCl (d), if applicable with their counterions. The used atomic numbering schemes are also shown.

(a)

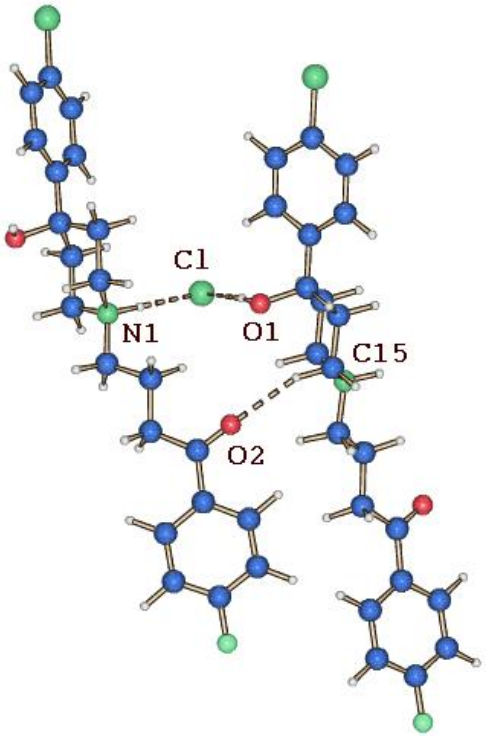

(b)

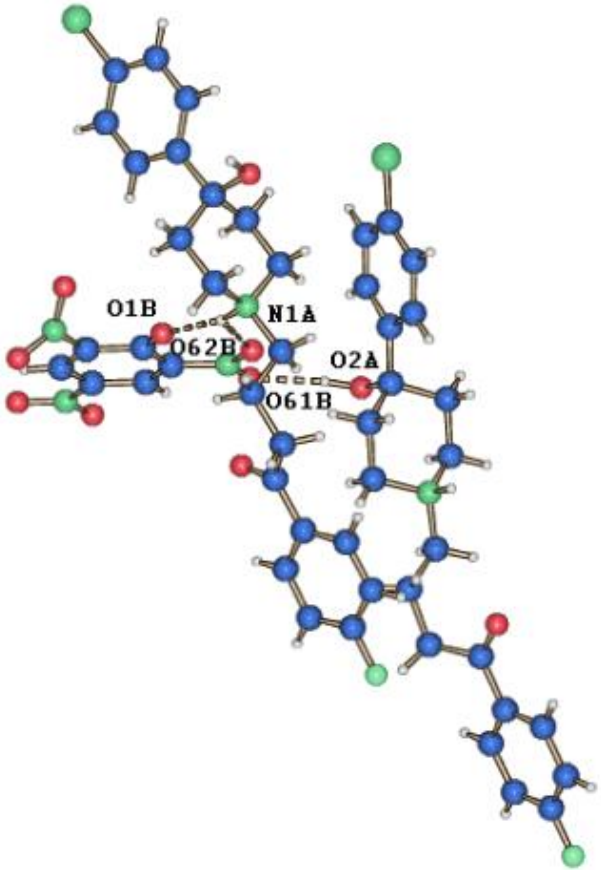

(c)

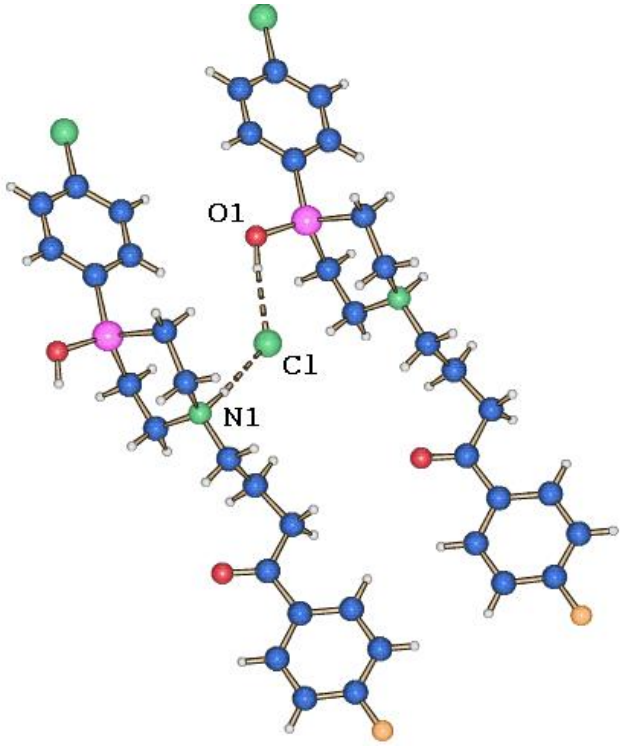

Fig. 4 Intermolecular hydrogen bonds of **1a**·HCl (a), **1a**·HPic (b) and **1b**·HCl (c) in the crystal, leading to a linkage between neighbored ammonium cations via the chloride (a,c) and picrate (b) counterion (SCHAKAL representations[39]).

(a)

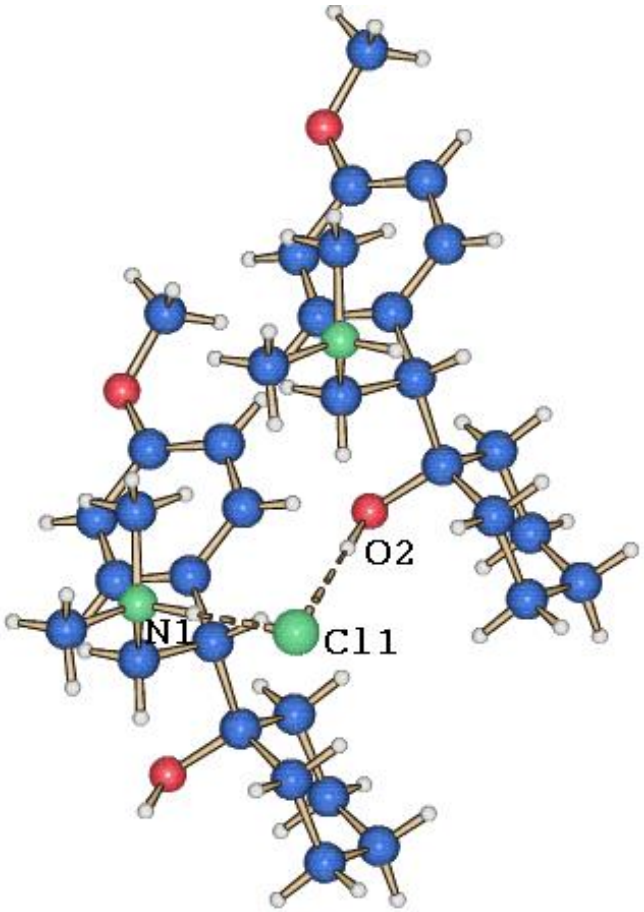

(b)

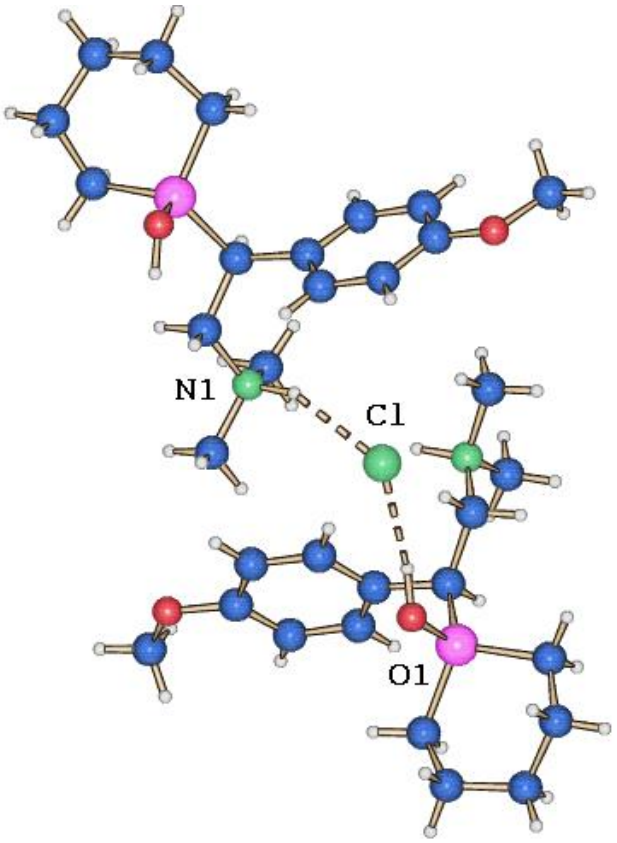

Fig. 5 Intermolecular hydrogen bonds of **2a**·HCl-ortho (a) and **2b**·HCl (b) in the crystal, leading to a linkage between neighbored ammonium cations via the chloride counterion (SCHAKAL representations[39]). The hydrogen bonding system of **2a**·HCl-mono (not shown) is comparable.

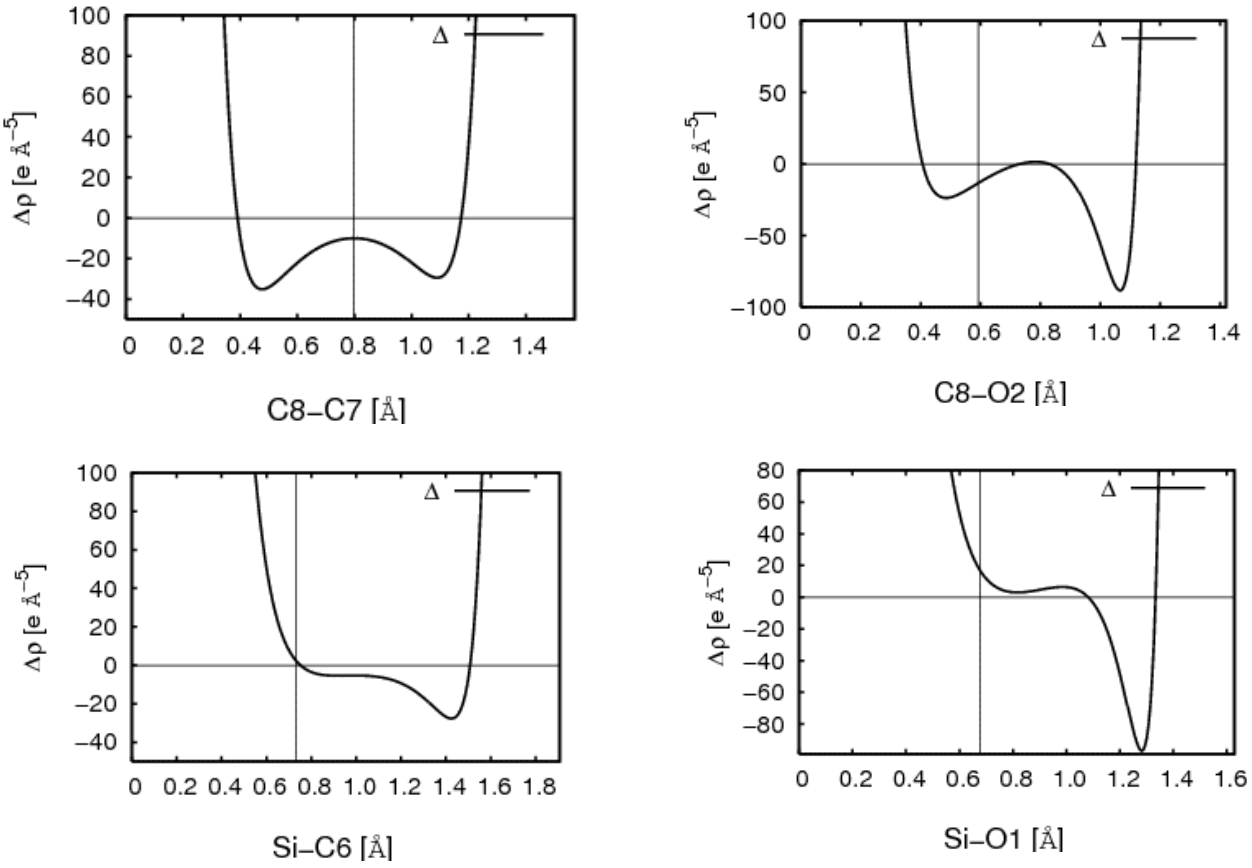

Fig. 6 Laplacian distributions along the C8–C7 and C8–O2 bonds in **2a**·HCl-ortho (above) and along the Si–C6 and Si–O1 bonds in **2b**·HCl (below).

(a)

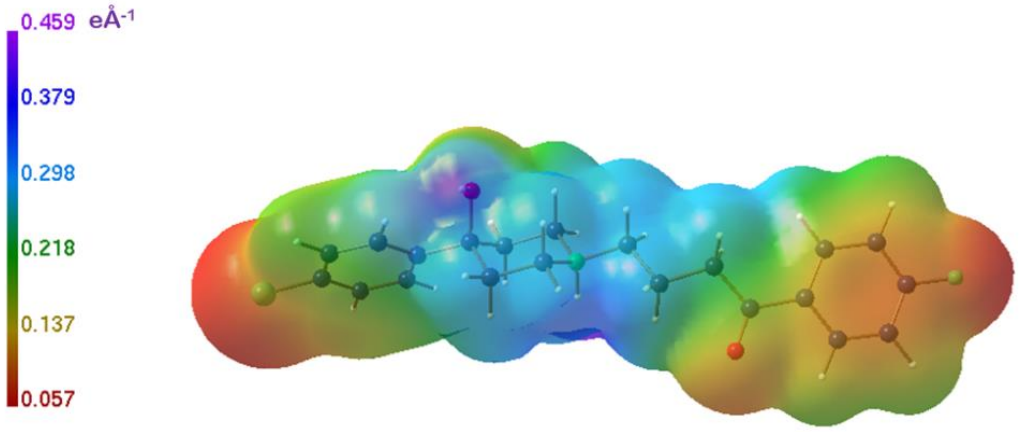

(b)

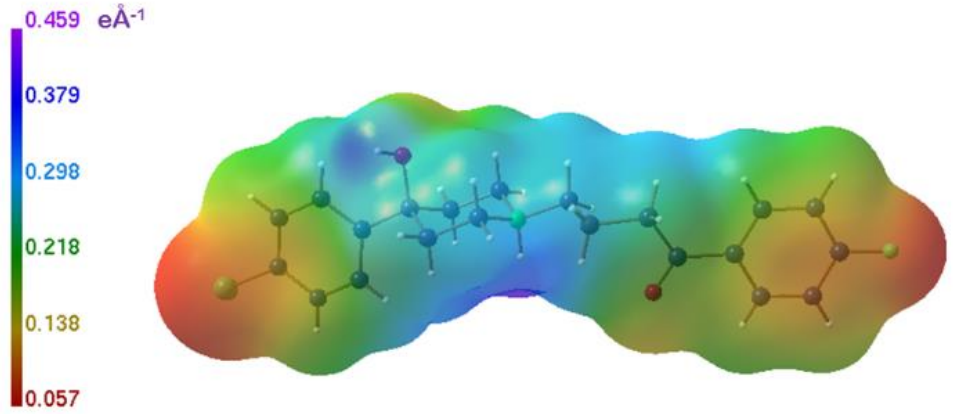

(c)

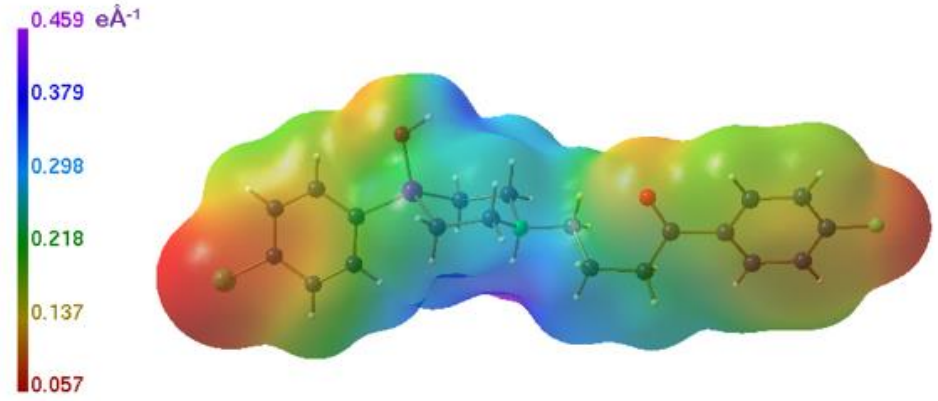

Fig. 7 Electrostatic potentials of the ammonium cations of **1a**·HCl (a), **1a**·HPic (b) and **1b**·HCl (c) mapped onto the isoelectron density surface ρ = 0.0067 e Å^{-3}.[31]

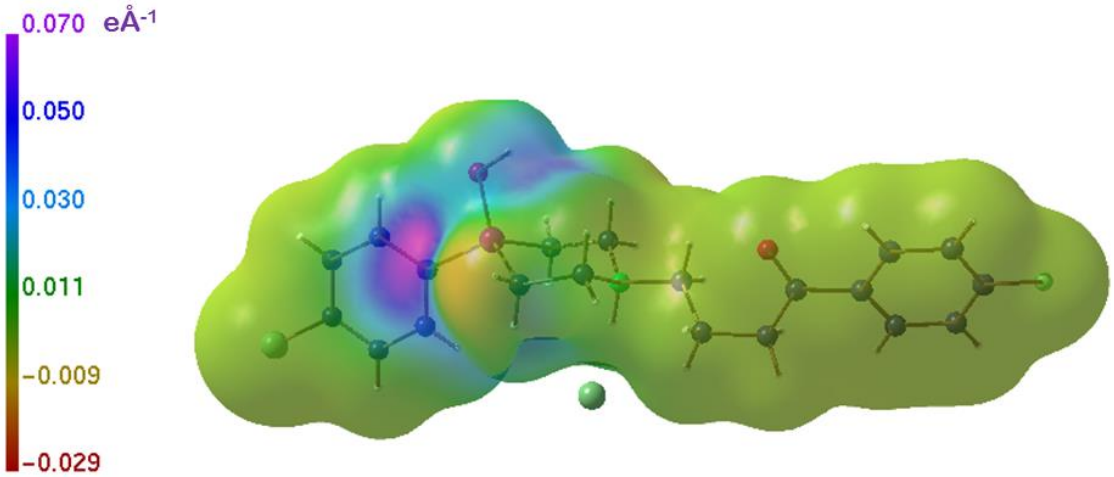

Fig. 8 Electrostatic difference potential **1b**·HCl/**1a**·HCl.[31]

(a)

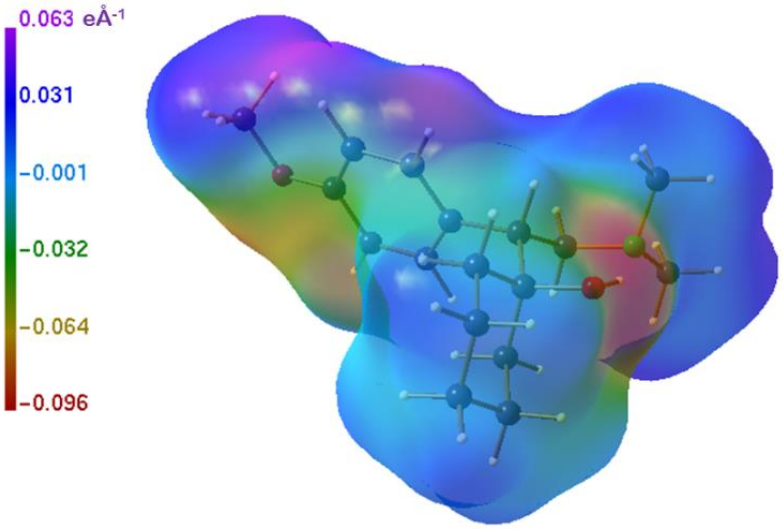

(b)

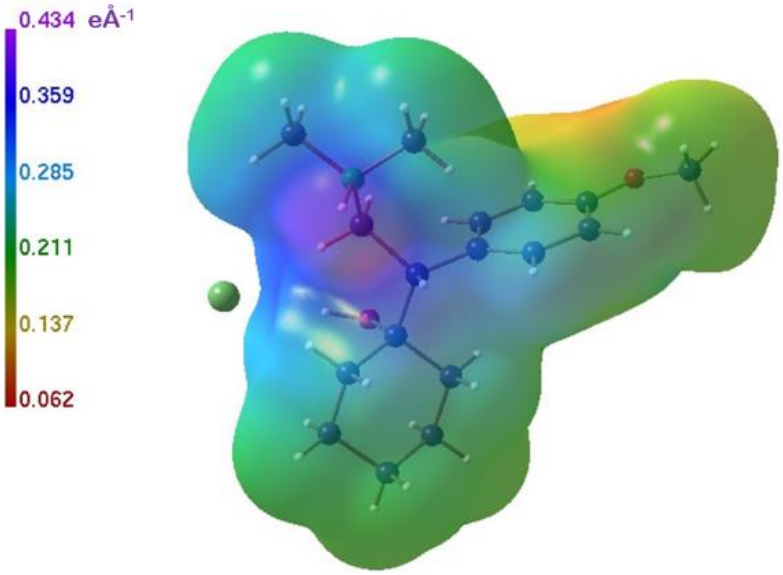

(c)

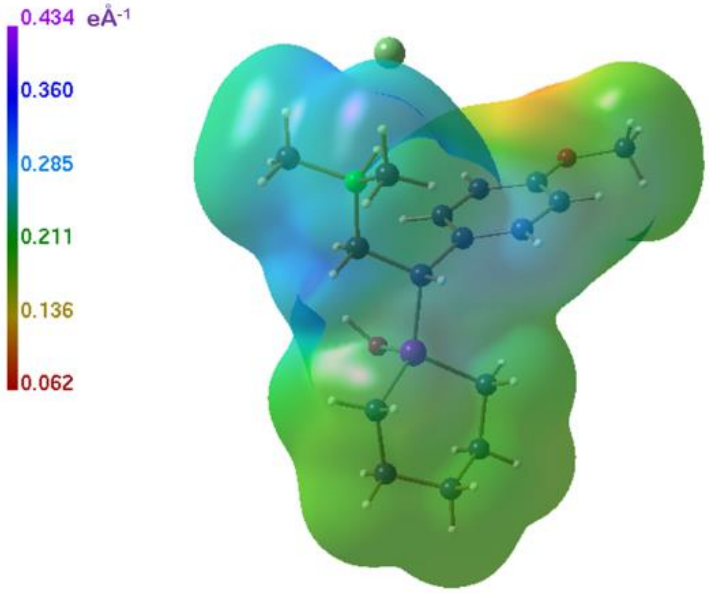

Fig. 9 Electrostatic potentials of **2a** (a), **2a**·HCl-ortho (b) and **2b**·HCl (c) mapped onto the isoelectron density surface ρ = 0.0067 e Å^{-3}.[31]

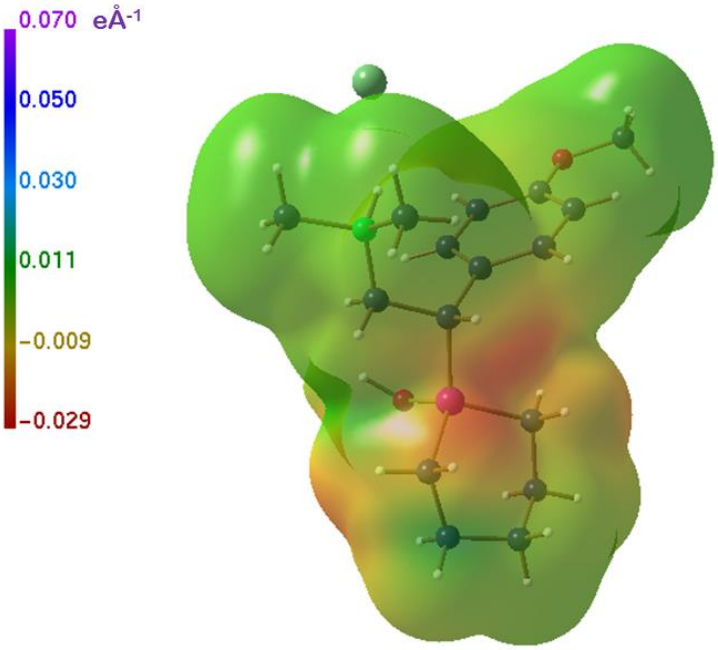

Fig.10 Electrostatic difference potential **2b**·HCl/**2a**·HCl-ortho.[31]

(a)

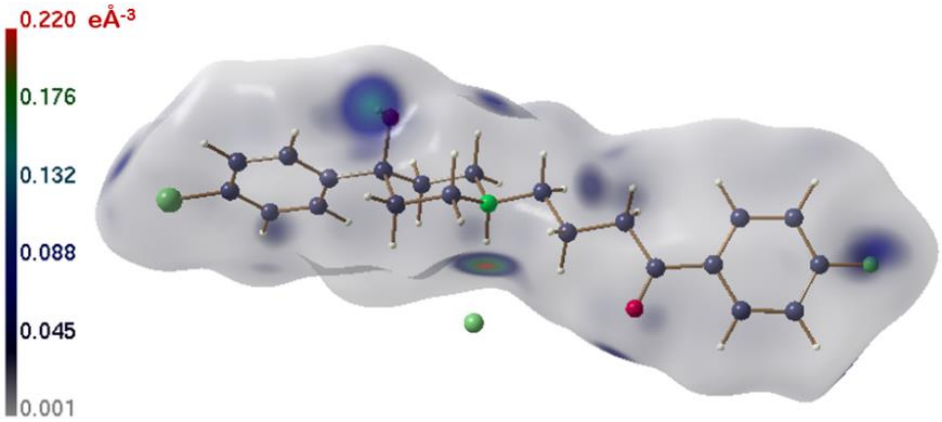

(b)

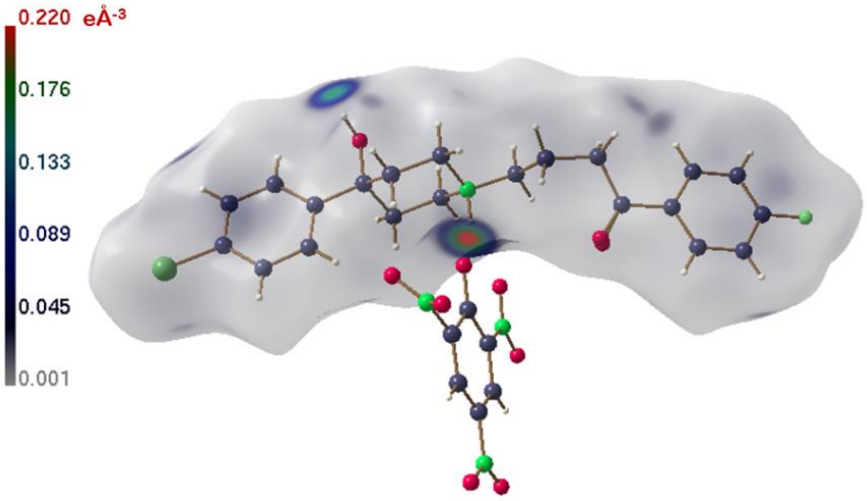

(c)

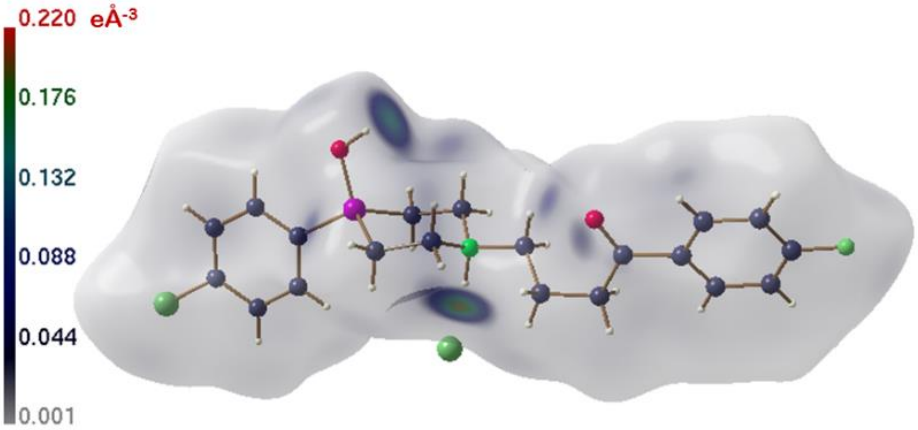

Fig. 11 Hirshfeld surfaces of **1a**·HCl (a), **1 a**·HPic (b) and **1b**·HCl (c).[31]

(a)

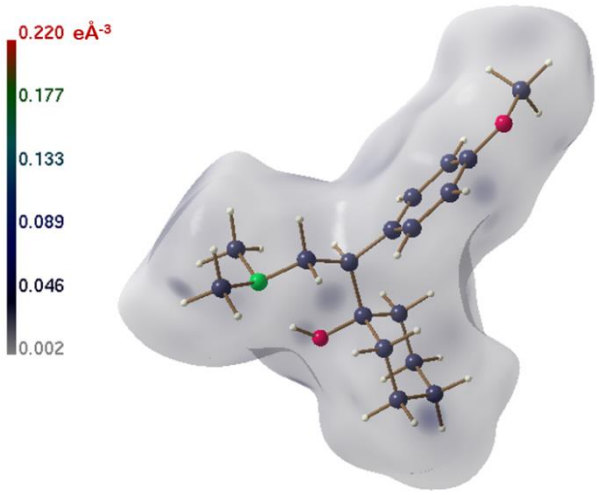

(b)

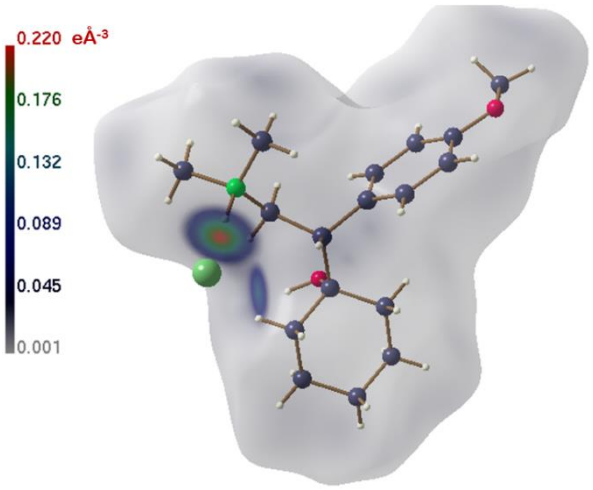

(c)

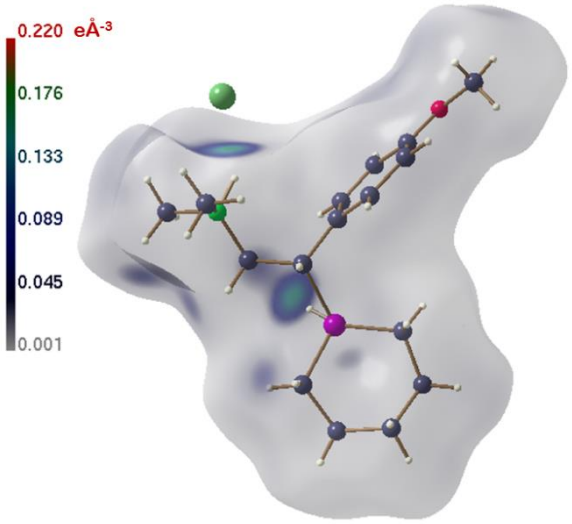

Fig. 12 Hirshfeld surfaces of **2a** (a), **2a**·HCl-mono (b) and **2b**·HCl (c).[31]

Table 1 Selected crystallographic and refinement data for **1a**·HCl, **1a**·HPic and **1b**·HCl[a]

Compound	**1a**·HCl	**1a**·HPic	**1b**·HCl
Formula	$C_{21}H_{24}Cl_2FNO_2$	$C_{27}H_{26}ClFN_4O_9$	$C_{20}H_{24}Cl_2FNO_2Si$
Crystal system	monoclinic	orthorhombic	triclinic
Space group (No.)	$P2_1/c$ (14)	$Pna2_1$ (33)	$P\bar{1}$ (2)
Z	4	4	2
V [Å^3]	1981.9(3)	2723.8(2)	1077.6(3)
$(\sin\theta/\lambda)_{max}$ [Å^{-1}]	0.64	0.76	0.63
Unique reflections	4168	7472	3895
Observed reflections [$F_o^2 \geq 2\sigma(F_o^2)$]	3660	5784	3096
Multipole refinement:			
$R(F)$	0.0300	0.0327	0.0339
$R_{all}(F)$	0.0351	0.0512	0.0453
$R_w(F)$	0.0268	0.0185	0.0265
$R(F^2)$	0.0419	0.0387	0.0489
$R_{all}(F^2)$	0.0425	0.0432	0.0510
$R_w(F^2)$	0.0537	0.0364	0.0526
Min/max $\Delta\rho$ [e Å^{-3}]	–0.506/0.604	–0.245/0.442	–0.208/0.484
Gof	3.09	1.49	2.14
N_{ref}/N_v	13.7	14.0	11.6

[a] For further data, see refs. 3a and 13.

Table 2 Selected crystallographic and refinement data for **2a**, **2a**·HCl-ortho, **2a**·HCl-mono and **2b**·HCl[a]

Compound	**2a**	**2a**·HCl-ortho	**2a**·HCl-mono	**2b**·HCl
Formula	$C_{17}H_{27}NO_2$	$C_{17}H_{28}ClNO_2$	$C_{17}H_{28}ClNO_2$	$C_{16}H_{28}ClNO_2Si$
Crystal system	monoclinic	orthorhombic	monoclinic	orthorhombic
Space group (No.)	$P2_1/n$ (14)	$Pca2_1$ (29)	$P2_1/n$ (14)	$Pca2_1$ (29)
Z	4	4	4	4
V [Å^3]	1566.9(7)	1766.0(6)	1740.9(19)	1787.7(4)
$(\sin\theta/\lambda)_{max}$ [Å^{-1}]	0.65	0.70	0.61	0.64
Unique reflections	3428	2474	3216	3825
Observed reflections $[F_o^2 \geq 2\sigma(F_o^2)]$	2600	1629	1422	3664
Multipole refinement:				
$R(F)$	0.0323	0.0408	0.0450	0.0229
$R_{all}(F)$	0.0595	0.1173	0.1465	0.0243
$R_w(F)$	0.0283	0.0254	0.0598	0.0204
$R(F^2)$	0.0345	0.0444	0.0719	0.0365
$R_{all}(F^2)$	0.0377	0.0748	0.0953	0.0367
$R_w(F^2)$	0.0567	0.0498	0.1186	0.0410
Min/max $\Delta\rho$ [e Å^{-3}]	–0.161/0.199	–0.222/0.222	–0.349/0.342	–0.136/0.203
Gof	1.51	2.02	1.49	2.42
N_{ref}/N_v	12.5	7.5	6.5	16.9

[a] For further data, see refs. 4b and 14–16.

Table 3 Summary of hydrogen bonding topologies of **1a**·HCl, **1a**·HPic and **1b**·HCl

Compound	D–H···A	D···A [Å]	H···A [Å]	$\rho(\mathbf{r}_{BCP})$ [e Å^{-3}]	$\nabla^2\rho(\mathbf{r}_{BCP})$ [e Å^{-5}]
1a·HCl	O1–H1···Cl[a]	3.194(1)	2.24(2)	0.13	1.88
1a·HCl	N1–HN···Cl[b]	3.038(1)	2.02(2)	0.21	2.71
1a·HCl	C15–H15B···O2[c]	3.324(1)	2.30(2)	0.08	1.08
1a·HPic	O2A–H2O···O61B[d]	2.841(2)	1.90(2)	0.15	2.66
1a·HPic	N1A–H1N···O1B[e]	2.703(1)	1.73(1)	0.24	3.85
1a·HPic	N1A–H1N···O62B[e]	3.008(1)	2.35(2)	0.06	1.08
1b·HCl	O1–H1···Cl[f]	3.149(2)	2.19(2)	0.14	1.96
1b·HCl	N1–HN···Cl[e]	3.077(2)	2.06(1)	0.19	2.49

[a] Symmetry code: 1 – *x*, 2 – *y*, –*z*.

[b] Symmetry code: 1 – *x*, 1/2 + *y*, 1/2 – *z*.

[c] Symmetry code: *x*, 5/2 – *y*, –1/2 + *z*.

[d] Symmetry code: 1/2 + *x*, 1/2 – *y*, *z*.

[e] Symmetry code: *x*, *y*, *z*.

[f] Symmetry code: –1 + *x*, *y*, *z*.

Table 4 Summary of hydrogen bond topologies of **2a, 2a**·HCl-ortho, **2a**·HCl-mono and **2b**·HCl

Compound	D–H···A	D···A [Å]	H···A [Å]	$\rho(\mathbf{r}_{BCP})$ [e Å^{-3}]	$\nabla^2\rho(\mathbf{r}_{BCP})$ [e Å^{-5}]
2a	O1–H1···N1[a]	2.713(1)	1.82(1)	0.22	2.97
2a·HCl-ortho	O2–H2B···Cl[a]	3.178(3)	2.22(2)	0.13	1.97
2a·HCl-ortho	N1–H1A···Cl[b]	3.046(3)	2.03(1)	0.21	2.66
2a·HCl-mono	O2–H27···Cl[c]	3.212(5)	2.28(2)	0.12	1.62
2a·HCl-mono	N1–H28···Cl[a]	3.034(6)	2.03(2)	0.21	2.70
2b·HCl	O1–HO···Cl[d]	3.119(1)	2.17(1)	0.15	2.05
2b·HCl	N1–HN···Cl[a]	3.064(1)	2.17(1)	0.16	2.15

[a] Symmetry code: *x*, *y*, *z*.

[b] Symmetry code: *x*, 1 + *y*, *z*.

[c] Symmetry code: 1 + *x*, *y*, *z*.

[d] Symmetry code: –*x*, –*y*, –1/2 + *z*.

Table 5 Averaged bond topological properties for **1a**·HCl, **1a**·HPic and **1b**·HCl

Bond	Length [Å]	$\rho(\mathbf{r}_{BCP})$ [e Å^{-3}]	$\nabla^2\rho(\mathbf{r}_{BCP})$ [e Å^{-5}]	ε[a]	N[b]	C–C bond order[c]
C–C (aromatic)	1.385(9)	2.16(5)	–18.2(12)	0.21(3)	36	1.67
C–C (single)	1.522(8)	1.71(2)	–11.5(4)	0.04(2)	18	1.07
Si–C[d]	1.864(8)	0.86(2)	+3.8(3)	0.06(3)	3	
(O=)C–C	1.498(15)	1.79(4)	–12.7(5)	0.08(3)	6	1.16
C=O[e]	1.213	2.95	–32.9	0.09	2	
C–O(H)	1.424	1.82	–13.1	0.04	2	
Si–O(H)[d]	1.623	1.01	+17.3	0.07	1	
C–N	1.500(8)	1.82(3)	–11.5(5)	0.01(1)	9	
C–F	1.339(3)	1.92(1)	–16.6(2)	0.01(1)	3	
C–Cl	1.732(10)	1.32(3)	–2.3(3)	0.06(2)	3	

[a] The ellipticity ε is defined by $(\lambda_1/\lambda_2) - 1$, with λ_1 and λ_2 being the two principal negative curvatures of $\rho(\mathbf{r})$ at a BCP and is a measure for the asphericity and hence the double bond character of a bond.

[b] N = number of entries contributing to the average.

[c] The bond order n_b was calculated as $n_b = \exp[C_1(\rho(\mathbf{r}_{BCP}) - C_2)]$, with $C_1 = 1.0229$ and $C_2 = 1.6459$.[40]

[d] Only **1b**·HCl.

[e] Not included for **1a**·HPic, because of disorder.

Table 6 Averaged bond topological properties for **2a, 2a**·HCl-ortho, **2a**·HCl-mono and **2b**·HCl

Bond	Length [Å]	$\rho(\mathbf{r}_{BCP})$ [e Å^{-3}]	$\nabla^2\rho(\mathbf{r}_{BCP})$ [e Å^{-5}]	ε[a]	N[b]	C–C bond order[c]
C–C (aromatic)	1.392(8)	2.14(2)	–17.5(7)	0.21(2)	24	1.65
C–C (single)	1.530(14)	1.68(4)	–10.8(8)	0.03(2)	33	1.04
Si–C[d]	1.88(3)	0.86(2)	+3.6(1)	0.05(1)	3	
C–N[e]	1.417(5)	1.70(1)	–6.2(1)	0.16(1)	3	
C–N[f]	1.494(9)	1.85(3)	–11.4(5)	0.01(1)	9	
C–O(H)[g]	1.430(9)	1.79(2)	–12.5(9)	0.03(1)	3	
Si–O(H)[h]	1.629	1.00	+16.8	0.02	1	
C(aromatic)–O	1.359(8)	2.08(2)	–18.6(10)	0.09(1)	4	
H_3C–O	1.413(9)	1.85(4)	–11.8(8)	0.02(1)	4	

[a] The ellipticity ε is defined by $(\lambda_1/\lambda_2) - 1$, with λ_1 and λ_2 being the two principal negative curvatures of $\rho(\mathbf{r})$ at a BCP and is a measure for the asphericity and hence the double bond character of a bond.

[b] N = number of entries contributing to the average.

[C] The bond order n_b was calculated as $n_b = \exp[C_1(\rho(\mathbf{r}_{BCP}) - C_2)]$, with $C_1 = 1.0229$ and $C_2 = 1.6459$.[40]

[d] Only **2b**·HCl**.**

[e] Only **2a** (neutral).

[f] Only **2a**·HCl-ortho, **2a**·HCl-mono and **2b**·HCl (charged).

[g] Only **2a, 2a**·HCl-ortho and **2a**·HCl-mono.

[h] Only **2b**·HCl.

Table 7 Atomic properties of **1a**·HCl/**1a**·HPic/**1b**·HCl (charges q and volumes V_{tot}). Only atoms with $|q| \geq 0.15$ e in either **1a**·HCl, **1a**·HPic or **1b**·HCl are listed.

Atom[a]	q [e]	V_{tot} [Å^3]
C1/Si	0.31/0.31/2.99	5.78/6.13/3.97
O1	–0.92/–0.93/–1.36	15.94/16.73/20.47
O2	–0.91/–[b]/–0.91	16.75/–[b]/18.44
Cl1	–1.18/–/–1.01	35.40/–/34.95
Cl2	–0.22/–0.22/–0.23	33.14/34.02/41.72
F	–0.58/–0.58/–0.59	17.51/18.49/19.77
N	–0.91/–0.81/–0.91	8.37/8.17/8.57
C7	–0.06/–0.05/–0.83	10.35/9.81/15.97
C13	–0.05/–0.02/–0.70	8.65/7.56/11.45
C14	0.17/0.19/0.18	7.85/7.73/7.42
C15	0.18/0.21/0.20	7.65/6.92/7.36
C16	–0.06/–0.03/–0.80	7.96/8.01/12.58
C17	0.16/0.20/0.21	8.09/7.61/7.21
C20	0.78/1.06[b]/0.79	7.94/6.66[b]/7.95
C24	0.43/0.46/0.43	8.88/7.90/10.31
HO[c]	0.62/0.58/0.59	1.63/2.19/2.08
HN[c]	0.60/0.50/0.48	1.37/1.99/2.29

[a] Atom numbering according to **1a**·HCl and **1b**·HCl; the data for **1a**·HPic refer to chemically equivalent atoms.

[b] Affected by disorder or disordered neighbor atoms.

[c] All further hydrogen atoms have charges and volumes in the range 0.05–0.14 e and 6–9 Å^3, respectively.

Table 8 Atomic properties of **2a**/**2a**·HCl-ortho/**2a**·HCl-mono/**2b**·HCl (charges q and volumes V_{tot}). Only atoms with $|q| \geq 0.15$ e in either **2a**, **2a**·HCl-ortho, **2a**·HCl-mono or **2b**·HCl are listed.

Atom[a]	q [e]	V_{tot} [Å^3]
C5/C8/Si	0.29/0.32/0.31/3.02	5.60/5.37/5.39/3.70
O1/O2/O1	–0.93/–0.94/–0.93/–1.37	14.52/14.64/14.89/18.76
O2/O1/O2	–0.91/–0.93/–0.93/–0.92	16.49/14.56/16.19/15.52
Cl1/Cl1/Cl	–/–1.01/–1.00/–1.00	–/38.28/37.36/37.10
N1/N1/N	–0.81/–0.87/–0.89/–0.89	9.88/8.43/8.64/8.42
C1/C15/C9	0.22/0.20/0.21/0.20	8.94/9.82/9.66/8.72
C2/C16/C8	0.22/0.19/0.21/0.20	8.93/9.52/8.61/9.78
C3/C14/C7	0.23/0.21/0.21/0.19	6.94/7.18/7.14/7.26
C4/C7/C6	0.01/0.02/0.03/–0.78	6.78/6.66/6.47/10.26
C6/C13/C5	–0.04/–0.03/–0.01/–0.81	7.71/7.55/7.53/12.30
C10/C9/C1	–0.05/–0.01/0.00/–0.81	8.29/7.33/7.78/12.12
C14/C4/C13	0.37/0.37/0.41/0.39	8.65/8.98/9.22/8.64
C17/C17/C16	0.34/0.39/0.38/0.37	9.68/9.55/8.37/9.37
HO[b]	0.54/0.56/0.56/0.59	2.16/2.23/2.39/2.01
HN[b]	–/0.48/0.47/0.48	–/2.26/2.46/2.82

[a] Atom numbering according to **2a**/**2a**·HCl-ortho = **2a**·HCl-mono/**2b**·HCl. Note: atomic numbering for **2a**·HCl-ortho and **2a**·HCl-mono is the same.

[b] All further hydrogen atoms have charges and volumes in the range 0.03–0.09 e and 6–10 Å^3, respectively.

1 For reviews dealing with silicon-containing drugs, see: (*a*) R. Tacke and H. Linoh, in *The Chemistry of Organic Silicon Compounds, Part 2*, ed. S. Patai, Z. Rappaport, Wiley-VCH, Chichester, 1989, pp. 1143–1206; (*b*) W. Bains and R. Tacke, *Curr. Opin. Drug. Discovery Dev.*, 2003, **6**, 526–543; (*c*) G. A. Showell and J. S. Mills, *Drug Discovery Today*, 2003, **8**, 551–556; (*d*) J. S. Mills and G. A Showell, *Expert Opin. Investig. Drugs,* 2004, **13**, 1149–1157; (*e*) P. K. Pooni and G. A Showell, *Mini-Rev. Med. Chem.*, 2006, **6**, 1169–1177; (*f*) S. McN. Sieburth and C.-A. Chen, *Eur. J. Org. Chem.*, 2006, 311–322; (*g*) S. Gately and R. West, *Drug Dev. Res.*, 2007, **68**, 156–163; (*h*) A. K. Franz, *Curr. Opin. Drug Discovery Dev.*, 2007, **10**, 654–671; (*i*) N. A. Meanwell, *J. Med. Chem.*, 2011, **54**, 2529–2591; (*j*) A. K. Franz and S. O. Wilson, *J. Med. Chem.*, 2013, **56**, 388–405; (*k*) S. McN. Sieburth, *Top. Med Chem.*, 2014; DOI: 10.1007/7355_2014_80; (*l*) R. Tacke and S. Dörrich, *Top. Med. Chem.*, 2014; DOI: 10.1007/7355_2014_55.

2 For recent studies on sila-substituted drugs, see: (*a*) J. B. Bauer, W. P. Lippert, S. Dörrich, D. Tebbe, C. Burschka, V. B. Christie, D. M. Tams, A. P. Henderson, B. A. Murray, T. B. Marder, S. A. Przyborski and R. Tacke, *ChemMedChem*, 2011, **6**, 1509–1517; (*b*) M. J. Barnes, C. Burschka, M. W. Büttner, R. Conroy, J. O. Daiss, I. C. Gray, A. G. Hendrick, T. L. Hong, D. Kuehn, D. J. Miller, J. S. Mills, P. Mitchell, J. G. Montana, P. A Muniandy, H. Rapley, G. A. Showell, D. Tebbe, R. Tacke, J. B. H. Warneck und B. Zhu, *ChemMedChem*, 2011, **6**, 2070–2080; (*c*) R. Tacke, R. Bertermann, C. Burschka, S. Dörrich, M. Fischer, B. Müller, G. Meyerhans, D. Schepmann, B. Wünsch, I. Arnason and R. Bjornsson *ChemMedChem*, 2012, **7**, 523–532; (*d*) J. B. G. Gluyas, C. Burschka, S. Dörrich, J. Vallet, H. Gronemeyer and R. Tacke, *Org. Biomol. Chem,* 2012, **10**, 6914–6929.

3 Sila-haloperidol: (*a*) R. Tacke, T. Heinrich, R. Bertermann, C. Burschka, A. Hamacher and M. U. Kassack, *Organometallics*, 2004, **23**, 4468–4477; (*b*) R. Tacke, F. Popp, B. Müller, B. Theis, C. Burschka, A. Hamacher, M. U. Kassack, D. Schepmann, B. Wünsch, U. Jurva and E. Wellner, *ChemMedChem*, 2008, **3**, 152–164; (*c*) R. Tacke, B. Nguyen, C. Burschka, W. P. Lippert, A. Hamacher, C. Urban and M. U. Kassack, *Organometallics*, 2010, **29**, 1652–1660; (*d*) T. Johansson, L. Weidolf, F. Popp, R. Tacke and U. Jurva, *Drug Metab. Dispos.*, 2010, **38**, 73–83.

4 Sila-venlafaxine: (*a*) J. O. Daiss, M. Penka, C. Burschka and R. Tacke, *Organometallics*, 2004, **23**, 4987–4994; (*b*) J. O. Daiss, C. Burschka, J. S. Mills, J. G. Montana, G. A. Showell, J. B. H. Warneck and R. Tacke, *Organometallics*, 2006, **25**, 1188–1198; (*c*) G. A. Showell, M. J.

Barnes, J. O. Daiss, J. S. Mills, J. G. Montana, R. Tacke and J. B. H. Warneck, *Bioorg. Med. Chem. Lett.*, 2006, **16**, 2555–2558; (*d*) J. B. H. Warneck, F. H. M. Cheng, M. J. Barnes, J. S. Mills, J. G. Montana, R. J. Naylor, M.-P. Ngan, M.-K. Wai, J. O. Daiss, R. Tacke and J. A. Rudd, *Toxicol. Appl. Pharmacol.*, 2008, **232**, 369–375.

5 P. A. J. Janssen, C. van de Westeringh, A. H. M. Jagenau, P. J. A. Demoen, B. K. F. Hermans, G. H. P. van Daele, K. H. L. Schellekens, C. A. M. van der Eycken and C. J. E. Niemegeers, *J. Med. Pharm. Chem.*, 1959, **1**, 281–297.

6 (*a*) D. F. Levinson, *Clin. Ther.*, 1991, **13**, 326–352; (*b*) D. E. Casey, *Int. Clin. Psychopharmacol.*, 1995, **10**, 105–114.

7 (*a*) B. Subramanyam, S. M. Pond, D. W. Eyles, H. A. Whiteford, H. G. Fouda and N. Castagnoli Jr., *Biochem. Biophys. Res. Commun*, 1991, **181**, 573–578; (*b*) W. Dauer and S. Przedborski, *Neuron*, 2003, **39**, 889–909.

8 (*a*) V. L. Ellingrod and P. J. Perry, *Am. J. Hosp. Pharm.,* 1994, **51**, 3033–3046; (*b*) E. Schweizer, R. J. Thielen and A. Frazer, *Exp. Opin. Invest. Drugs,* 1997, **6**, 65–78; (*c*) R. L. Rudolph, *Acta Psychiatr. Scand.*, 2002, **106** (Suppl. 415), 24–30; (*d*) H. Sauer, S. Huppertz-Helmhold and W. Dierkes, *Pharmacopsychiatry*, 2003, **36**, 169–175; (*e*) M. A. Gutierrez, G. L. Stimmel and J. Y. Aiso, *Clin. Ther.*, 2003, **25**, 2138–2154.

9 P. Luger, M. Weber, C. Hübschle and R. Tacke, *Org. Biomol. Chem*., 2013, **11**, 2348–2354.

10 B. Dittrich, T. Koritsánszky and P. Luger, *Angew. Chem. Int. Ed.*, 2004, **43**, 2718–2721.

11 B. Dittrich, C. B. Hübschle, K. Pröpper, F. Dietrich, T. Stolper and J. J. Holstein, *Acta Crystallogr.*, 2013, **B69**, 91–104.

12 F. H. Allen, *Acta Crystallogr.*, 2002, **B58**, 380–388.

13 J. P. Jasinski, R. J. Butcher, Q. N. M. Hakim Al-Arique, H. S. Yathirajan and B. Narayana, *Acta Crystallogr.*, 2009, **E65**, o2403–o2404.

14 L. Tessler and I. Goldberg, *Acta Crystallogr.*, 2004, **E60**, o1868–o1869.

15 D. Vega, D. Fernández and G. Echeverria, *Acta Crystallogr.*, 2000, **C56**, 1009–1010.

16 A. Sivalakshmidevi, K. Vyas, S. M. Rao and G. O. Reddy, *Acta Crystallogr.*, 2002, **E58**, o1072–o1074.

17 N. K. Hansen and P. Coppens, *Acta Crystallogr.*, 1978, **A34**, 909–921.

18 C. B. Hübschle, P. Luger and B. Dittrich, *J. Appl. Crystallogr.*, 2007, **40**, 623–627.

19 A. Volkov, P. Macchi, L. J. Farrugia, C. Gatti, P. R. Mallinson, T. Richter and T. Koritsánszky, *XD2006 – a computer program for multipole refinement, topological analysis of charge*

densities and evaluation of intermolecular energies from experimental and theoretical structure factors, University of Buffalo, NY, USA; University of Milano, Italy; University of Glasgow, UK; CNRISTM, Milano, Italy; Middle Tennessee State University, TN, USA, 2006.

20 C. B. Hübschle and B. Dittrich, *J. Appl. Crystallogr.*, 2011, **44**, 238–240.

21 *(a)*B. Dittrich, T. Koritsansky, A. Volkov, S. Mebs and P. Luger, *Angew. Chem. Int. Ed.* 2007, **46**, 2935-2938; *(b)* K. Pröpper, J. J. Holstein, C. B. Hübschle, C. S. Bond and B. Dittrich, *Acta Crystallogr.*, 2013, **D659**, 1530–1539.

22 R. F. W. Bader, in *Atoms in Molecules – A Quantum Theory*, Clarendon Press, Oxford, UK, 1990.

23 C. K. Johnson, ORTEP Report ORNL-3794, Oak Ridge National Laboratory, Oak Ridge, TN, USA, 1965.

24 A. L. Spek, *Acta Crystallogr.*, 2009, **D65**, 148–155.

25 S. Grabowsky, Ph.D. Thesis, 2009, Freie Universität Berlin, Germany; see http://www.diss.fu-berlin.de/diss/receive/FUDISS_thesis_000000015999.

26 S. Grabowsky, M. F. Hesse, C. Paulmann, P. Luger and J. Beckmann, *Inorg. Chem*., 2009, **48**, 4384–4393.

27 S. Grabowsky, J. Beckmann, P. Luger, *Aust. J. Chem*., 2012, **65**, 785–795.

28 A. Volkov, C. Gatti, Y. Abramov and P. Coppens, *Acta Crystallogr.*, 2000, **A56**, 252-258.

29 *(a)* B. Pedersen, G. Wagner and R. Herrmann, ECHET98, https://www.ch.ic.ac.uk/ectoc/echet98/pub/048/index.htm; *(b)* N. Kocher, J. Henn, B. Gostevskii, D. Kost, I. Kalikhman, B. Engels and D. Stalke, *J. Amer. Chem. Soc.* 2004, **126**, 5563-5568; *(c)* H. Ott, Ch. Däschlein, D.Leusser, D. Schildbach, T. Seibel, D. Stalke and C. Strohmann, *J. Amer. Chem. Soc.* 2008, **130**, 11901-11911.

30 A. Volkov, H. F. King, P. Coppens and L. J. Farrugia, *Acta Crystallogr.*, 2006, **A62**, 400-408.

31 C. B. Hübschle and P. Luger, *J. Appl. Crystallogr.*, 2006, **39**, 901–904.

32 J. J. McKinnon, A. S. Mitchell and M. A. Spackman, *Chem. Eur. J.*, 1998, **4**, 2136–2141.

33 M. A. Spackman, J. J. McKinnon and D. Jayatilaka, *CrystEngComm.*, 2008, **10**, 377–388.

34 S. Scheins, M. Messerschmidt, W. Morgenroth, C. Paulmann and P. Luger, *J. Phys. Chem. A*, 2007, **111**, 5499–5508.

35 A. Bondi, *J. Phys. Chem.*, 1964, **68**, 441–451.

36 A. Bach, D. Lentz and P. Luger, *J. Phys. Chem. A*, 2001, **105**, 7405-7412.

37 C. F. Matta, N. Castillo, R. J. Boyd, *J. Phys. Chem. A*, 2005, **109**, 3669-3681.

38 *(a)* B. Dittrich, M. Weber, R. Kalinowski, S. Grabowsky, C. B. Hübschle and P. Luger, *Acta Crystallogr.*, 2009, **B65**, 749-756; *(b)* D. M. M. Jaradat, S. Mebs, L Chęcińska and P. Luger, *Carbohyd. Res.,* 2007, **342**, 1480–1489; *(c)* S. Grabowsky, R. Kalinowski, M. Weber, D. Förster, C. Paulmann and P. Luger, *Acta Crystallogr.*, 2009, **B65,** 488–501.

39 E. Keller and J. S. Pierrard, *SCHAKAL99*, University of Freiburg, Germany, 1999.

40 P. Luger, M. Messerschmidt, S. Scheins and A. Wagner, *Acta Crystallogr.*, 2004, **A60**, 390–396.